Restrictions on the Validity of the Thermal Conditions at the Porous-Fluid Interface—An Exact Solution

Kun Yang
School of Energy and Power Engineering,
Huazhong University of Science and Technology,
Wuhan 430074, P. R. China;
Department of Mechanical Engineering,
University of California, Riverside,
Riverside, CA 92521-0425

Kambiz Vafai[1]
Department of Mechanical Engineering,
University of California, Riverside,
Riverside, CA 92521-0425
e-mail: vafai@engr.ucr.edu

Thermal conditions at the porous-fluid interface under local thermal nonequilibrium (LTNE) conditions are analyzed in this work. Exact solutions are derived for both the fluid and solid temperature distributions for five of the most fundamental forms of thermal conditions at the interface between a porous medium and a fluid under LTNE conditions and the relationships between these solutions are discussed. This work concentrates on restrictions, based on the physical attributes of the system, which must be placed for validity of the thermal interface conditions. The analytical results clearly point out the range of validity for each model for the first time in the literature. Furthermore, the range of validity of the local thermal equilibrium (LTE) condition is discussed based on the introduction of a critical parameter. The Nusselt number for the fluid at the wall of a channel that contains the fluid and porous medium is also obtained. The effects of the pertinent parameters such as Darcy number, Biot number, Bi, Interface Biot number, Bi_{int}, and fluid to solid thermal conductivity ratio are discussed. [DOI: 10.1115/1.4004350]

Keywords: thermal condition, porous-fluid interface, local thermal nonequilibrium

1 Introduction

Due to its wide range of engineering applications, convective heat transfer in porous media has gained increased interest in recent years. These applications include geothermal engineering, heat pipes, solid matrix heat exchangers, electronics cooling, enhanced oil recovery, thermal insulation, and chemical reactors. Among which, thermal convection in composite systems is an important aspect. This system consists partly of a porous region and partly of an open region. One example is a channel with a partially filled porous medium. Poulikakos and Kazmierczak [1] studied fully developed forced convection in a channel, where the porous matrix was attached at the channel wall but did not extent throughout the channel. The results showed that there was a critical value of porous region thickness at which the Nusselt number reaches a minimum. Chikh et al. [2] investigated forced convection between two concentric cylinders where the inner cylinder is exposed to a constant heat flux, a porous layer is attached to the inner cylinder and the porous material does not extend across the full annulus. It was also found that there exists a critical thickness of the porous layer at which heat transfer is minimum in the case of low thermal conductivity materials; however, this was not observed for the highly conducting materials. Alkam and Al-Nimr [3] presented a method to improve the thermal performance of a conventional concentric tube heat exchanger by inserting high-thermal conductivity porous substrates on both sides of the inner tube wall. Mohamad [4] numerically investigated heat transfer enhancement in a pipe or a channel with the porous medium partially filling the core of the conduit. It was found that this method can enhance the rate of heat transfer, while the pressure drop is much less than that for a conduit fully filled with a porous medium. Pavel and Mohamad [5] experimentally investigated the problem of air flowing inside a pipe when different porous media are emplaced at the core of the pipe. The results showed that a partial filling has the advantage of a comparable increase in the Nusselt number and a smaller increase in the pressure drop. Kim et al. [6] numerically investigated forced convection in a circular pipe partially filled with a porous medium, which included two types of configurations (in two separate cases). It was found that there exists a critical porous layer thickness where the Nu reaches a minimum in one case and a maximum for another case. Satyamurty and Bhargavi [7] studied forced convection in the thermally developing region of a channel where a partially filled porous medium was attached to one wall only. Kuznetsov [8] has obtained some solutions for the velocity and temperature distributions for few composite systems.

Different types of interfacial conditions between a porous medium and a fluid layer have been presented in the literature [1–12]. Beavers and Joseph [9] first presented a velocity interfacial condition based on a slip velocity proportional to the exterior velocity gradient, which was shown to be in reasonable agreement with experimental results. References [1–8] utilized continuity in both the temperature and heat flux at the interface. Vafai and Thiyagaraja [10] presented a detailed analytical solution for the velocity and temperature distributions, as well as the Nusselt number distribution, for three general and fundamental interfaces, namely, the interface between two different porous media, the interface between a fluid region and a porous medium and the interface between an impermeable medium and a porous medium. Vafai and Kim [11] first derived an exact solution for the fluid mechanics of the interface region between a porous medium and a fluid layer, accounting for both boundary and inertial effects. Alazmi and Vafai [12] comprehensively analyzed five fundamental hydrodynamic interface conditions and four thermal interface conditions. It was shown that the variance within different models have a negligible effect on the results for most practical applications.

There are two primary ways for representing heat transfer in a porous medium, LTE model and LTNE model. The LTE model is more convenient to use, and it is utilized by the above-mentioned references [1–8,10,12]. However, the temperature difference

[1]Corresponding author.

Contributed by the Heat Transfer Division of ASME for publication in the Journal of Heat Transfer. Manuscript received January 10, 2011; final manuscript received May 22, 2011; published online September 16, 2011. Assoc. Editor: Darrell W. Pepper.

between the fluid and solid phases within the porous media may be significant and the assumption of local thermal equilibrium is not valid for some applications. Therefore, the LTNE model has been analyzed in the past [13–17]. Because there are two regions with different temperatures, namely, the solid and fluid phase temperatures of the porous region and the fluid temperature of the fluid region, the use of the LTNE model requires an additional thermal interfacial condition. Ochoa-Tapia and Whitaker [18] developed the heat flux jump conditions between a porous medium and a homogeneous fluid based on a volume averaging theorem, in which an excess surface heat exchange term was introduced to control the total heat flux distribution between the solid and fluid phases within the porous region. However, either experimental studies or numerical experiments are needed to determine the excess surface heat transfer coefficient. The presented work has applications in various areas [19–24]. Five of the most fundamental forms of thermal conditions at the interface between a porous medium and a fluid under LTNE condition are analyzed, leading to a presentation of exact solutions for all of the analyzed conditions. The work concentrates on the restrictions based on the physical attributes of the system that must be placed for the validity of the thermal interface conditions. The analytical results clearly point out the range of validity for each model in terms of the pertinent physical parameters. This is the first time that the existence of restrictions on the validity of the thermal conditions at the porous–fluid interface has been established. This is crucial, as the inappropriate use of the interface conditions can lead to substantial errors. Furthermore, the range of validity of the LTE condition is discussed based on the introduction of a critical parameter.

2 Modeling and Formulation

The problem under consideration is shown schematically in Fig. 1. Fluid flows through a rectangular channel partially filled with a porous medium subject to a constant heat flux boundary condition. The height of the channel is $2H$, the height of the porous medium is $2H_1$ and the heat flux applied at the wall is q_w. The following assumptions are invoked in the analyzing this problem.

(1) The flow is steady and incompressible.
(2) Natural convection and radioactive heat transfer are negligible.
(3) Fully developed heat and flow fields are considered and fluid flow through the porous medium is represented by the Darcian flow model.
(4) Properties such as porosity, specific heat, density and thermal conductivity are assumed to be constant.

Based on these assumptions, the governing conservation equations are written separately for the porous and open regions. For the porous region, the energy equations are obtained from the works of Amiri and Vafai [13,14] employing the local thermal nonequilibrium model.

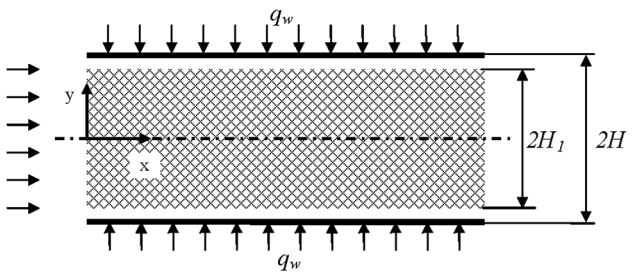

Fig. 1 Schematic diagram for flow through a channel partially filled with a porous medium and the corresponding coordinate system

Fluid phase

$$k_{f,\text{eff}}\frac{\partial^2 T_f}{\partial y^2} + h_i\alpha(T_s - T_f) = \rho c_p u\frac{\partial T_f}{\partial x} \tag{1}$$

Solid phase

$$k_{s,\text{eff}}\frac{\partial^2 T_s}{\partial y^2} - h_i\alpha(T_s - T_f) = 0 \tag{2}$$

where T_f and T_s are the fluid and solid temperatures, u the fluid velocity, $k_{f,\text{eff}}$, and $k_{s,\text{eff}}$ the effective fluid and solid thermal conductivities, respectively, ρ and c_p the density and specific heat of the fluid, h_i the interstitial heat transfer coefficient, and α is the interfacial area per unit volume of the porous medium.

The momentum equation in the porous region is

$$-\frac{\mu_f}{K}u - \frac{dp}{dx} = 0 \tag{3}$$

where K denotes the permeability, μ_f the fluid dynamic viscosity, and p the pressure.

For the open region the momentum and energy equations, respectively, are

$$-\frac{dp}{dx} + \mu_f\frac{d^2u}{dy^2} = 0 \tag{4}$$

$$k_f\frac{\partial^2 T_f}{\partial y^2} = \rho c_p u\frac{\partial T_f}{\partial x} \tag{5}$$

The boundary conditions for this problem are

$$\left.\frac{\partial u}{\partial y}\right|_{y=0} = 0 \tag{6}$$

$$\left.\frac{\partial T_f}{\partial y}\right|_{y=0} = \left.\frac{\partial T_s}{\partial y}\right|_{y=0} = 0 \tag{7}$$

$$u|_{y=H} = 0 \tag{8}$$

$$k_f\left.\frac{\partial T_f}{\partial y}\right|_{y=H} = q_w \tag{9}$$

$$\left.\frac{\partial u}{\partial y}\right|_{y=H_1^+} = \frac{\alpha^*}{\sqrt{K}}(u_B - u_p) \tag{10}$$

which is the slip velocity condition at the interface between the open and porous regions based on Beavers and Joseph [9], where u_B denotes the interface velocity, u_p the velocity in the porous medium, α^* the velocity slip coefficient, which is a dimensionless quantity depending on the material.

In this work, we develop five models to describe the temperature interface conditions between the open and porous regions. These are models A, B (composed of three sub models: B.1, B.2, and B.3), and C. The interface conditions for these models are given below:

2.1 Model A. When the heat transfer between the fluid and solid phases at the interface is large enough, their temperatures are equal at the interface. That is

$$T_f|_{y=H_1^-} = T_s|_{y=H_1^-} = T_f|_{y=H_1^+} \tag{11}$$

$$k_{f,\text{eff}}\left.\frac{\partial T_f}{\partial y}\right|_{y=H_1^-} + k_{s,\text{eff}}\left.\frac{\partial T_s}{\partial y}\right|_{y=H_1^-} = k_f\left.\frac{\partial T_f}{\partial y}\right|_{y=H_1^+} = q_i \tag{12}$$

where q_i is the heat flux at the interface, which represents the heat energy transferred through the porous region.

2.2 Model B. For most cases, the heat transfer between the fluid and solid phases at the interface is not large enough, thus their temperatures are not equal at the interface. Therefore, a interface thermal parameter, β, is introduced to evaluate the total heat flux distribution between the solid and fluid phases at the interface in Model B.

$$T_f\big|_{y=H_1^-} = T_f\big|_{y=H_1^+} \tag{13}$$

$$k_f \left.\frac{\partial T_f}{\partial y}\right|_{y=H_1^+} = q_i \tag{14}$$

$$k_{f,\,\mathrm{eff}} \left.\frac{\partial T_f}{\partial y}\right|_{y=H_1^-} = \beta q_i \tag{15}$$

$$k_{s,\,\mathrm{eff}} \left.\frac{\partial T_s}{\partial y}\right|_{y=H_1^-} = (1-\beta) q_i \tag{16}$$

where β is the ratio of heat flux for the fluid phase to the total heat flux at the interface. The ratio β can be calculated based on the following three different methods.

$$\text{Model B.1 } \beta_1 = \frac{k_{f,\mathrm{eff}}}{k_{f,\mathrm{eff}} + k_{s,\mathrm{eff}}} \tag{17.1}$$

$$\text{Model B.2 } \beta_2 = \frac{k_f}{k_f + k_s} \tag{17.2}$$

$$\text{Model B.3 } \beta_3 = \varepsilon \tag{17.3}$$

where ε denotes porosity, k_f and k_s the fluid and solid thermal conductivities, respectively.

2.3 Model C. The temperatures of fluid and solid phases are considered not to be equal at the interface, and the heat flux jump interfacial condition presented by Ochoa-Tapia and Whitaker [18] is utilized as the basis for Model C, in which a interface heat transfer coefficient, h_{int}, is introduced to calculate the heat exchange between fluid and solid phases at the interface.

$$T_f\big|_{y=H_1^-} = T_f\big|_{y=H_1^+} \tag{18}$$

$$k_f \left.\frac{\partial T_f}{\partial y}\right|_{y=H_1^+} = q_i \tag{19}$$

$$k_{f,\,\mathrm{eff}} \left.\frac{\partial T_f}{\partial y}\right|_{y=H_1^-} = q_i - h_{\mathrm{int}}\left(T_f\big|_{y=H_1^-} - T_s\big|_{y=H_1^-}\right) \tag{20}$$

$$k_{s,\,\mathrm{eff}} \left.\frac{\partial T_s}{\partial y}\right|_{y=H_1^-} = h_{\mathrm{int}}\left(T_f\big|_{y=H_1^-} - T_s\big|_{y=H_1^-}\right) \tag{21}$$

To normalize the governing equations, boundary conditions and interface conditions, the following dimensionless variables are introduced

$$\theta = \frac{k_{s,\mathrm{eff}}(T - T_{s,i})}{q_w H} \qquad \eta = \frac{y}{H} \qquad \eta_1 = \frac{H_1}{H}$$
$$k = \frac{k_{f,\mathrm{eff}}}{k_{s,\mathrm{eff}}} \qquad k_1 = \frac{k_f}{k_{s,\mathrm{eff}}} \qquad Bi = \frac{h_i \alpha H^2}{k_{s,\mathrm{eff}}}$$
$$Bi_{\mathrm{int}} = \frac{h_{\mathrm{int}} H}{k_{s,\mathrm{eff}}} \qquad Da = \frac{K}{H^2} \qquad U = \frac{u}{-\frac{H^2}{\mu_f}\frac{dp}{dx}}$$
$$\gamma = \frac{q_i}{q_w} \tag{22}$$

where $T_{s,i}$ is the temperature for solid phase at the interface and Bi is the Biot number which represents the ratio of the conduction resistance of the solid phase to the heat exchange resistance between the fluid and solid phases [16].

Adding governing Eqs. (1) and (2), and integrating the resultant equation from the center to the fluid-porous interface and applying the corresponding boundary and interface conditions, the following equation is obtained.

$$\rho c_p u_p \frac{\partial T_f}{\partial x} = \frac{q_i}{H_1} \tag{23}$$

By integrating Eq. (5) from the interface to the wall and applying the corresponding boundary and interface conditions, the following equation is obtained.

$$\rho c_p u_{m,\mathrm{open}} \frac{\partial T_f}{\partial x} = \frac{q_w - q_i}{H - H_1} \tag{24}$$

where $u_{m,\mathrm{open}}$ is the average fluid velocity within the open region.

Based on the work of Beavers and Joseph [9], the solutions for momentum Eqs. (3) and (4) and the corresponding boundary and interface conditions (6), (8), and (10) are obtained as

For the porous region:

$$U = Da \quad 0 \le \eta \le \eta_1 \tag{25}$$

For the open region:

$$U = -0.5(\eta - \eta_1)^2 + \frac{\alpha^*}{\sqrt{Da}}(U_B - Da)(\eta - \eta_1) + U_B \quad \eta_1 < \eta \le 1 \tag{26}$$

where U_B is the dimensionless interface velocity

$$U_B = \frac{0.5(1-\eta_1)^2 + \alpha^*\sqrt{Da}(1-\eta_1)}{1 + \frac{\alpha^*}{\sqrt{Da}}(1-\eta_1)} \tag{27}$$

The dimensionless average velocity within the open region is calculated as

$$U_{m,\mathrm{open}} = -\frac{1}{6}(1-\eta_1)^2 + \frac{\alpha^*}{2\sqrt{Da}}(U_B - Da)(1-\eta_1) + U_B \tag{28}$$

The dimensionless average velocity over the channel cross section is calculated as

$$U_m = \eta_1 Da + (1-\eta_1) U_{m,\mathrm{open}} \tag{29}$$

Based on Eqs. (22)–(25), (28) and Eq. (29), the dimensionless heat flux at the interface is derived as

$$\gamma = \frac{q_i}{q_w} = \frac{\eta_1 Da}{U_m} \tag{30}$$

2.4 Temperature Solution for Interface Condition of Model A. Using Eqs. (22)–(30), the energy equations and the corresponding boundary and interface conditions for Model A can be rewritten as

$$k\frac{\partial^2 \theta_f}{\partial \eta^2} + Bi(\theta_s - \theta_f) = \frac{\gamma}{\eta_1} \quad 0 \le \eta \le \eta_1 \tag{31}$$

$$\frac{\partial^2 \theta_s}{\partial \eta^2} - Bi(\theta_s - \theta_f) = 0 \quad 0 \le \eta \le \eta_1 \tag{32}$$

$$k_1 \frac{\partial^2 \theta_f}{\partial \eta^2} = \frac{U}{U_m} \quad \eta_1 < \eta \le 1 \tag{33}$$

$$\left.\frac{\partial\theta_f}{\partial\eta}\right|_{\eta=0} = \left.\frac{\partial\theta_s}{\partial\eta}\right|_{\eta=0} = 0 \tag{34}$$

$$\theta_f\big|_{\eta=\eta_1^-} = \theta_s\big|_{\eta=\eta_1^-} = \theta_f\big|_{\eta=\eta_1^+} = 0 \tag{35}$$

$$\left.\frac{\partial\theta_f}{\partial\eta}\right|_{\eta=1} = \frac{1}{k_1} \tag{36}$$

Utilizing the two coupled governing Eqs. (31) and (32), the following governing equations for the fluid and solid temperatures of porous region are obtained.

$$k\theta_f'''' - (1+k)Bi\theta_f'' = -Bi\frac{\gamma}{\eta_1} \tag{37}$$

$$k\theta_s'''' - (1+k)Bi\theta_s'' = -Bi\frac{\gamma}{\eta_1} \tag{38}$$

By utilizing the boundary and interface conditions (34) and (35) in Eqs. (31) and (32), the following equations are obtained.

$$\theta_f''(\eta_1^-) = \frac{\gamma}{\eta_1 k} \quad \theta_s''(\eta_1^-) = 0 \tag{39}$$

$$\theta_f''(0) = \theta_s''(0) = 0 \tag{40}$$

The temperature distribution for porous region is found by solving Eqs. (37) and (38) and applying the boundary Eqs. (34), (35), (39), and (40). The resultant equations are

$$\theta_f = \frac{\gamma}{(1+k)\eta_1}\left\{\frac{1}{2}\left(\eta^2-\eta_1^2\right) + \frac{1}{(1+k)Bi}\left[\frac{\cosh(\lambda\eta)}{\cosh(\lambda\eta_1)} - 1\right]\right\} \tag{41}$$

$$\theta_s = \frac{\gamma}{(1+k)\eta_1}\left\{\frac{1}{2}\left(\eta^2-\eta_1^2\right) + \frac{k}{(1+k)Bi}\left[1 - \frac{\cosh(\lambda\eta)}{\cosh(\lambda\eta_1)}\right]\right\} \tag{42}$$

where,

$$\lambda = \sqrt{Bi(1+k)/k} \tag{43}$$

The temperature distribution for open region is found by solving Eq. (33) and applying the boundary Eqs. (35) and (36). The resultant equations are

$$\theta_f = D_0(\eta-\eta_1)^4 + D_1(\eta-\eta_1)^3 + D_2(\eta-\eta_1)^2 + D_3(\eta-\eta_1) \tag{44}$$

where

$$\begin{aligned} D_0 &= -\frac{1}{24U_m k_1} \\ D_1 &= \frac{\alpha^*}{6U_m k_1\sqrt{Da}}(U_B - Da) \\ D_2 &= \frac{U_B}{2U_m k_1} \\ D_3 &= \frac{1}{k_1} - 4D_0(1-\eta_1)^3 - 3D_1(1-\eta_1)^2 - 2D_2(1-\eta_1) \end{aligned} \tag{45}$$

2.5 Temperature Solution for Interface Condition of Model B. The interface conditions for Model B can be rewritten as

$$\theta_s\big|_{\eta=\eta_1^-} = 0 \tag{46}$$

$$\left.\frac{\partial\theta_f}{\partial\eta}\right|_{\eta=\eta_1^-} = \frac{\beta\gamma}{k} \tag{47}$$

$$\theta_f\big|_{\eta=\eta_1^-} = \theta_f\big|_{\eta=\eta_1^+} \tag{48}$$

The temperature distribution is found by solving governing Eqs. (31)–(33) and applying the boundary and interface condition Eqs. (34), (36), and (46)–(48). This results in

For porous region

$$\theta_f = \frac{\gamma}{(1+k)\lambda\sinh(\lambda\eta_1)}[\beta - k(1-\beta)]\left[\frac{\cosh(\lambda\eta)}{k} + \cosh(\lambda\eta_1)\right] + \frac{\gamma\left(\eta^2-\eta_1^2\right)}{2\eta_1(1+k)} - \frac{\gamma}{(1+k)\eta_1 Bi} \tag{49}$$

$$\theta_s = \frac{\gamma}{(1+k)\lambda\sinh(\lambda\eta_1)}[\beta - k(1-\beta)][\cosh(\lambda\eta_1) - \cosh(\lambda\eta)] + \frac{\gamma\left(\eta^2-\eta_1^2\right)}{2\eta_1(1+k)} \tag{50}$$

For open region

$$\theta_f = D_0(\eta-\eta_1)^4 + D_1(\eta-\eta_1)^3 + D_2(\eta-\eta_1)^2 + D_3(\eta-\eta_1) + \theta_f\left(\eta_1^-\right) \tag{51}$$

where $\theta_f\left(\eta_1^-\right)$ can be calculated using Eq. (49), D_0, D_1, D_2, and D_3 can be calculated using Eq. (45).

2.6 Temperature Solution for Interface Condition of Model C. The interface conditions for Model C can be rewritten as

$$\theta_s\big|_{\eta=\eta_1^-} = 0 \tag{52}$$

$$k\left.\frac{\partial\theta_f}{\partial\eta}\right|_{\eta=\eta_1^-} = \gamma - Bi_{\text{int}}\left(\theta_f\big|_{\eta=\eta_1^-} - \theta_s\big|_{\eta=\eta_1^-}\right) \tag{53}$$

$$\theta_f\big|_{\eta=\eta_1^-} = \theta_f\big|_{\eta=\eta_1^+} \tag{54}$$

The temperature distribution is found by solving governing Eqs. (31)–(33) and applying the boundary and interface condition Eqs. (34), (36), and (52)–(54). This results in

For porous region

$$\theta_f = \frac{\gamma D_4}{\lambda^2\eta_1}\cosh(\lambda\eta) + \frac{\gamma\eta^2}{2\eta_1(1+k)} + \gamma\eta_1 D_5 \tag{55}$$

$$\theta_s = \frac{\gamma D_6}{\lambda^2\eta_1}\cosh(\lambda\eta) + \frac{\gamma\eta^2}{2\eta_1(1+k)} + \gamma\eta_1 D_7 \tag{56}$$

where

$$\begin{aligned} D_4 &= \frac{Bi\eta_1 + Bi_{\text{int}}}{\lambda k^2\sinh(\lambda\eta_1) + Bi_{\text{int}}k(1+k)\cosh(\lambda\eta_1)} \\ D_5 &= \frac{D_4 k^2}{Bi\eta_1^2(1+k)}\cosh(\lambda\eta_1) - \frac{1}{Bi\eta_1^2(1+k)} - \frac{1}{2(1+k)} \\ D_6 &= \frac{D_8 Bi_{\text{int}}\eta_1(1+k) - 1}{\sinh(\lambda\eta_1)(1+k)}\lambda\eta_1 \\ D_7 &= -\frac{D_6}{\lambda^2\eta_1^2}\cosh(\lambda\eta_1) - \frac{1}{2(1+k)} \\ D_8 &= \frac{D_4}{\lambda^2\eta_1^2}\cosh(\lambda\eta_1) + \frac{1}{2(1+k)} + D_5 \end{aligned} \tag{57}$$

For open region

$$\theta_f = D_0(\eta-\eta_1)^4 + D_1(\eta-\eta_1)^3 + D_2(\eta-\eta_1)^2 + D_3(\eta-\eta_1) + \theta_f\left(\eta_1^-\right) \tag{58}$$

where $\theta_f(\eta_1^-)$ can be calculated using Eq. (55), D_0,D_1, D_2, and D_3 can be calculated using Eq. (45).

3 Results and Discussion

3.1 Validity of the Interface Thermal Models. In order to satisfy the second law of thermodynamics, the dimensionless fluid phase temperature at the interface should be larger than the dimensionless solid phase temperature at the interface, that is

$$\theta_f|_{\eta=\eta_1^-} \geq \theta_s|_{\eta=\eta_1^-} \tag{59}$$

Substituting Eqs. (49) and (50) in Eq. (59), results in

$$1 \geq \beta \geq \beta_{cr} \tag{60}$$

where, β_{cr} denotes critical ratio of heat flux for the fluid phase to the total heat flux at the interface, which represents the minimum ratio of heat flux for the fluid phase to the total heat flux at the interface.

$$\beta_{cr} = \frac{\dfrac{\sinh(\lambda\eta_1)}{\lambda\eta_1\cosh(\lambda\eta_1)} + k}{1+k} \tag{61}$$

Critical heat flux ratio β_{cr} distributions for different parameters Bi and k are shown in Fig. 2. It is found that β_{cr} increases as η_1 and Bi become smaller or k becomes larger. When $Bi = 0.1$ and $k = 10$, β_{cr} is very close to 1, which means most of the heat flux at the interface is transferred through the fluid phase of the porous medium. When η_1 approaches zero, β_{cr} approaches 1, and again most of the heat flux at the interface is transferred through the fluid phase. Utilizing condition (60), the validity of Eq. (17) can be assessed.

(a) It should be noted that $\beta_{cr} \geq \beta_1$, and only when λ approaches infinity, β_{cr} approaches β_1. Based on condition (60) and Eq. (43), this means that the β_1 is valid when Bi approaches infinity.

(b) The effective thermal conductivity of the fluid and solid phases of porous media can be represented by

$$k_{f,\text{eff}} = \varepsilon k_f \tag{62}$$

$$k_{s,\text{eff}} = (1-\varepsilon)k_s \tag{63}$$

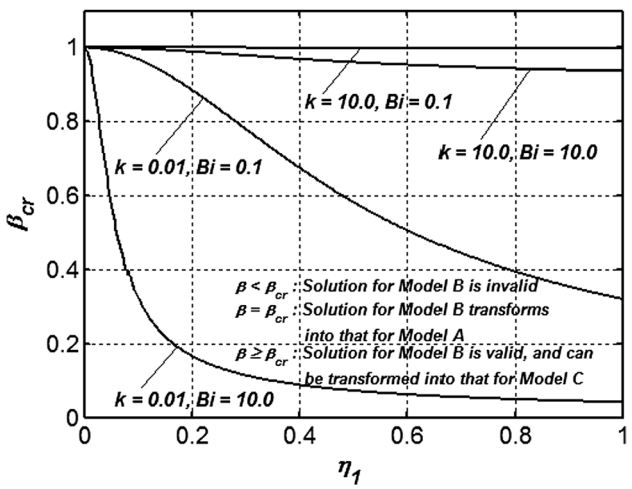

Fig. 2 β_{cr} distributions for different parameters Bi and k

Substituting Eqs. (62) and (63) in Eq. (17.2), which uses only k_f and k_s and not $k_{f,\text{eff}}$ and $k_{s,\text{eff}}$, results in

$$\beta_2 = \frac{k}{k + \frac{\varepsilon}{1-\varepsilon}} \tag{64}$$

When $\varepsilon > 0.5$, $\beta_2 < \beta_{cr}$. This means that β_2 is not valid for $\varepsilon > 0.5$.

(c) β_3 is valid for $\varepsilon \geq \beta_{cr}$

3.2 Equivalence Correlations Between Different Interface Thermal Models. Comparison of the solutions for Model A, Model B, and Model C, reveals some interesting physical features. It is found that these solutions can be transformed between each other as described below

(a) When $\beta = \beta_{cr}$, the temperatures of fluid and solid phases at the interface will be equal, thus the solution for Model B will transform into the solution for Model A.

(b) When $\beta = 1 - D_8 Bi_{\text{int}}\eta_1$, the solution for Model B will transform into the solution for Model C.

(c) When $Bi_{\text{int}} \to \infty$, the temperatures of fluid and solid phases at the interface will be equal, thus the solution for Model C will transform into the solution for Model A, and the solid phase at the interface will get the maximum fraction of the total heat flux at the interface, which is equal to $1 - \beta_{cr}$.

(d) When $Bi_{\text{int}} \to 0$, the heat exchange between fluid and solid phases at the interface vanish, thus the solution for Model C will transform into the solution for Model B for $\beta = 1$.

3.3 Temperature Results and the Validity of the LTE Condition. The dimensionless temperature distributions for Model A for different pertinent parameters η_1, Bi, and k are shown in Fig. 3. It should be noted that, based on the above-mentioned discussion, these temperatures are also the solutions for Model B for $\beta = \beta_{cr}$ and the solutions for model C for $Bi_{\text{int}} \to \infty$. When Bi is small, which translates into a weak internal heat transfer between the fluid and solid phases, the temperature difference between the two phases is relatively large, as shown in Figs. 3(*b*) and 3(*c*). However, when η_1 decreases, the temperature difference between the two phases is quite small, even for a small Bi, as shown in Figs. 3(*e*)–3(*f*). The reason for this phenomena is that, when η_1 is small, the heat flux at the interface is also small, as shown in Fig. 4. This means that only a small proportion of the imposed heat flux at the boundary is transferred into porous region, thus the influences of Bi and k can be negligible. From Eq. (30), it is found that the heat flux distributions at the interface is mainly dependent on Da and η_1, and independent of Bi and k. As can be seen in Fig. 4, when Da increases, more energy will be transferred through the porous region, thus the properties of the porous medium will have more influence on the temperature distributions. The dimensionless temperature distributions for Model C are shown in Fig. 5. Comparing Figs. 3(*a*)–3(*d*) and 5, it is found the temperature difference between fluid and solid phases at the interface increases as Bi_{int} becomes smaller. Different Bi_{int} will result different temperature distributions within the porous region. When $Bi_{\text{int}} \to \infty$, the solid phase temperature is always larger than that of the fluid phase within the porous region except the porous-fluid interface, where the temperature of solid phase is equal to that of the fluid phase. However, when Bi_{int} doesn't approach infinity, the fluid phase temperature is larger than that of the solid phase within the part of the porous region near the interface, and smaller than that of the solid phase within the other part of the porous region, as shown in Fig. 5. This results a changing of the direction of heat exchange between the solid and fluid phases.

The maximum relative temperature difference between solid and fluid phases within the porous region is computed as follows:

$$\%\Delta\theta = \frac{\max|\theta_s - \theta_f|}{\theta_f|_{\eta=1} - \theta_f|_{\eta=0}} \times 100 \tag{65}$$

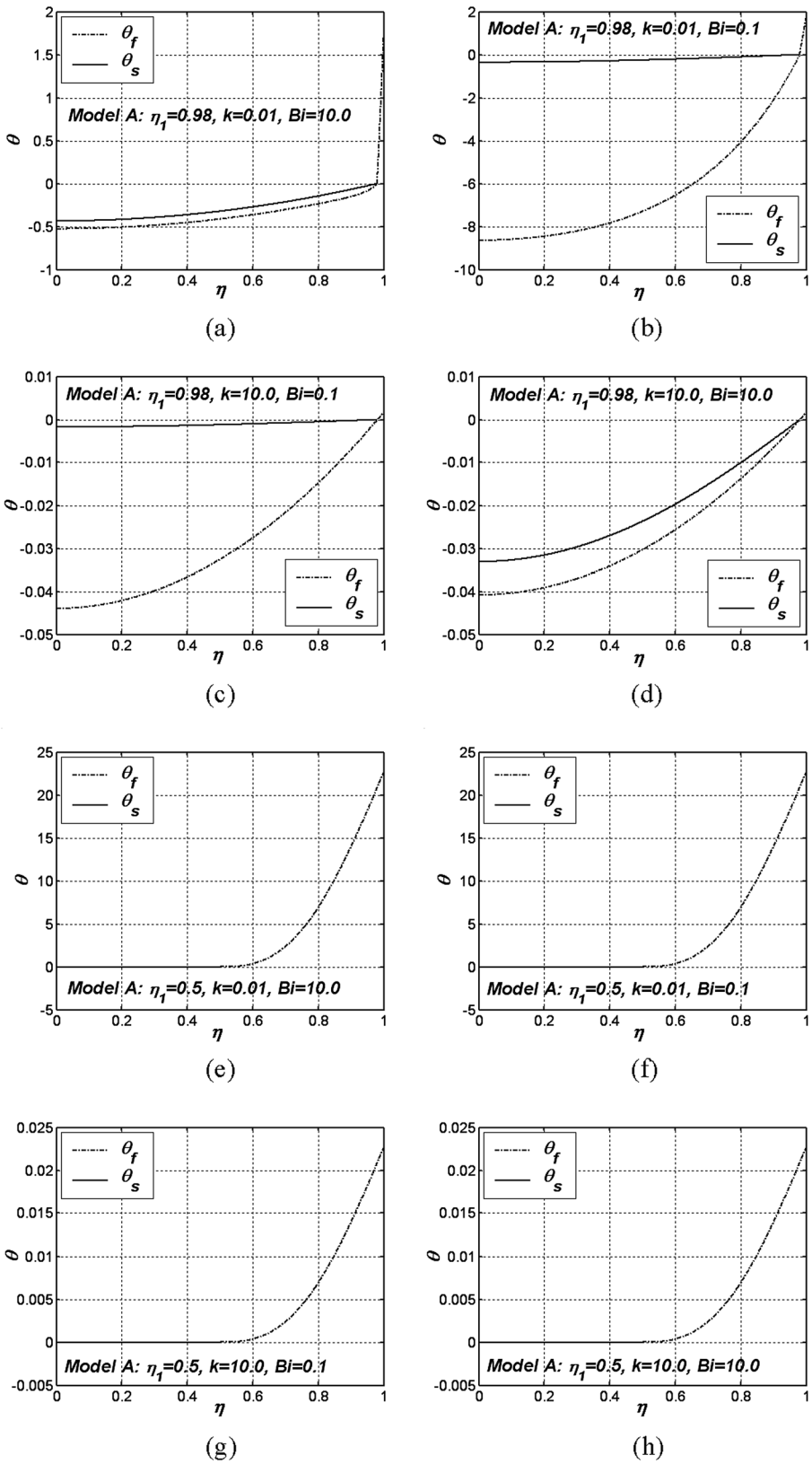

Fig. 3 Dimensionless temperature distributions for Model A for $\alpha^* = 0.78$, $Da = 1\times10^{-5}$, and $\varepsilon = 0.9$

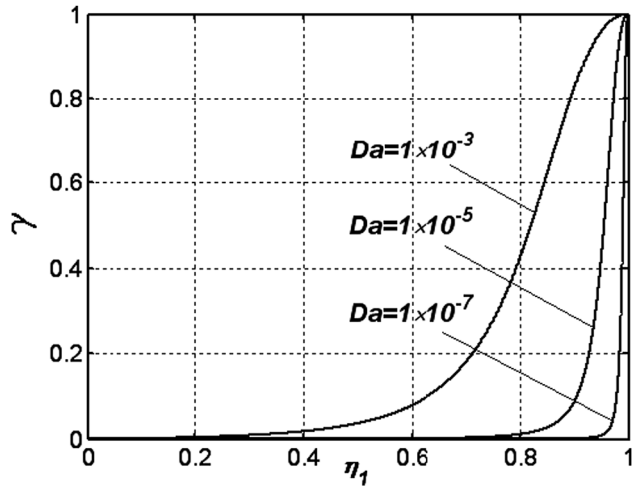

Fig. 4 Dimensionless heat flux distributions at the interface for $\alpha^* = 0.78$

The variable $\%\Delta\theta$ varies as a function of η_1 as shown in Fig. 6. This figure reveals that the maximum relative temperature difference between solid and fluid phases increases as η_1 and Da become larger. To examine the LTE condition, a critical $\eta_{1,cr}$ is introduced (as displayed in Fig. 7), at which the maximum relative temperature difference between solid and fluid phases within the porous region is within a small percentage difference. This small percentage difference is chosen to be 2%. That is

$$\%\Delta\theta|_{\eta_1=\eta_{1,cr}} = 2.0 \tag{66}$$

Figure 6 demonstrates that

(a) when $\eta_1 > \eta_{1,cr}$, $\%\Delta\theta > 2.0$, thus the LTE condition is considered to be invalid;
(b) when $\eta_1 < \eta_{1,cr}$, $\%\Delta\theta < 2.0$, thus the LTE condition is considered to be valid.

Figure 7 displays $\eta_{1,cr}$ variations as a function of pertinent parameters k,Bi,Bi_{int}, and Da. It is found that $\eta_{1,cr}$ increases as Bi becomes larger or k becomes smaller. When η_1 is small enough, the LTE condition is valid even for a small Bi, which can translates into a weak internal heat transfer between the fluid and solid phases. On the other hand, when η_1 is large enough, the LTE condition is not valid even for a large Bi. When Da becomes small, $\eta_{1,cr}$ will increase. The reason for this is that less energy will be transferred into the porous region as Da decreases. Comparing between Figs. 7(*a*) and 7(*b*), it is found that Bi_{int} has an important influence on $\eta_{1,cr}$. For example, when $k = 0.01$ and $Bi = 10$, different Bi_{int} will result in quite different $\eta_{1,cr}$ distributions.

3.4 Nusselt Number Results. The nondimensional bulk mean temperature of the fluid can be calculated as

$$\theta_{f,b} = \frac{\int_0^1 \theta_f(\eta) U d\eta}{U_m} \tag{67}$$

The wall heat transfer coefficient is obtained from

$$h_w = \frac{q_w}{T_{f,w} - T_{f,b}} \tag{68}$$

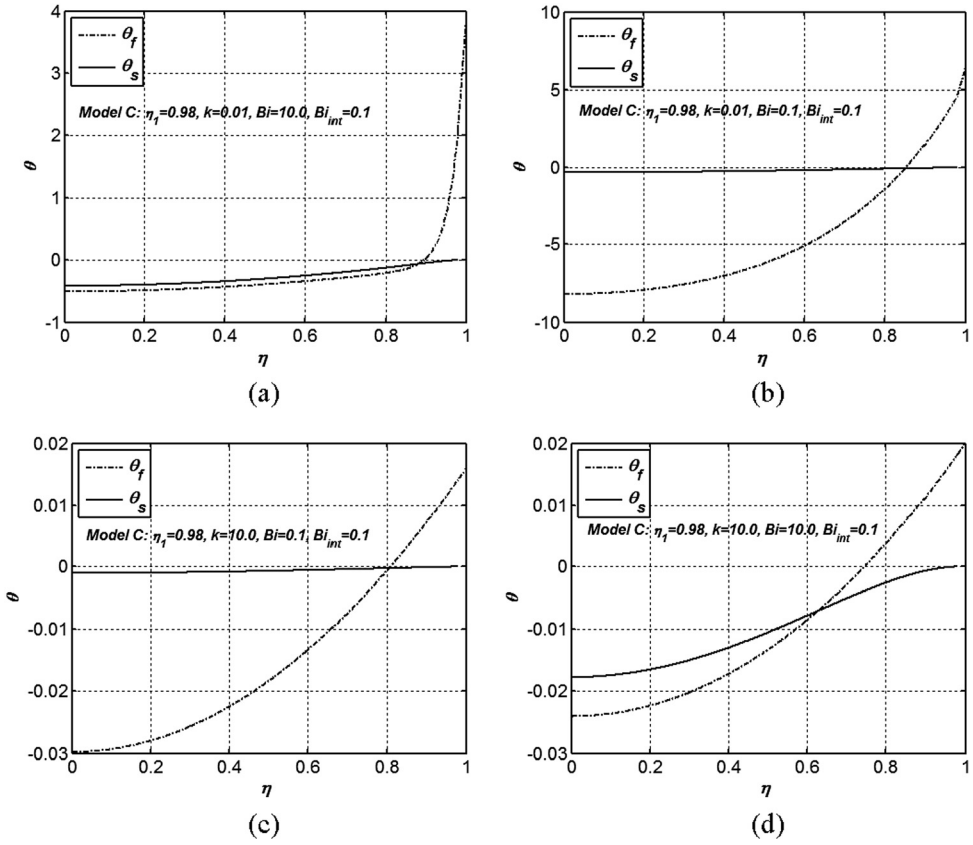

Fig. 5 Dimensionless temperature distributions for Model C for $\alpha^* = 0.78$, $Da = 1\times10^{-5}$, and $\varepsilon = 0.9$

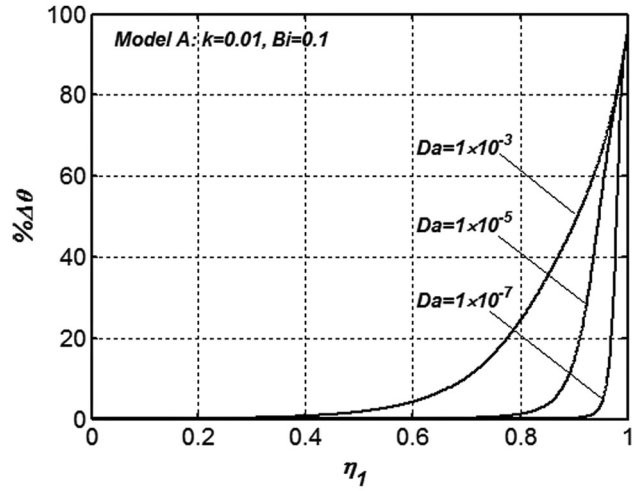

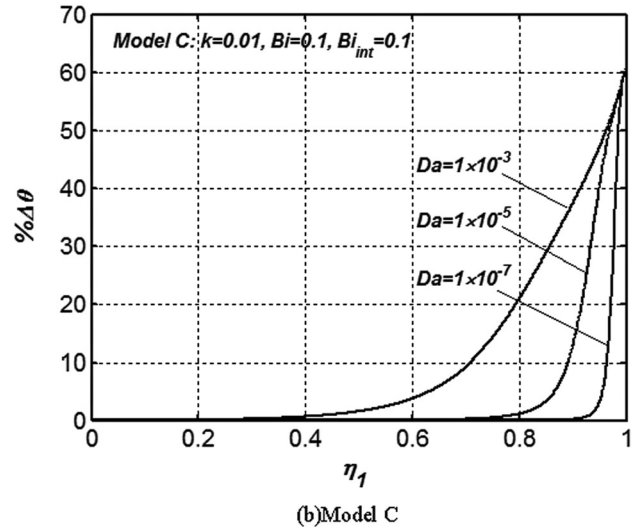

Fig. 6 $\%\Delta\theta$ **variations as a function of** η_1 **for** $\alpha^* = 0.78$ **and** $\varepsilon = 0.9$

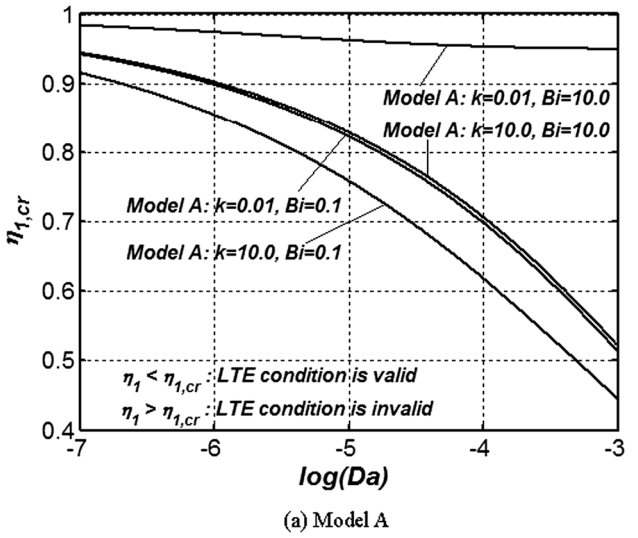

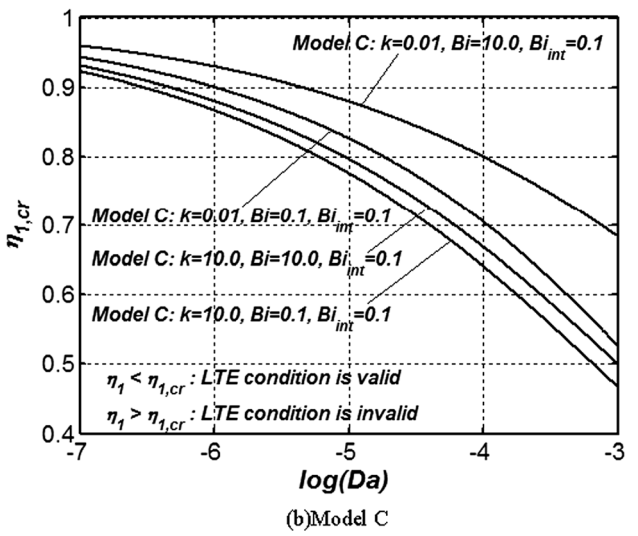

Fig. 7 $\eta_{1,cr}$ **variations as a function of pertinent parameters** k, Bi, Bi_{int}, **and** Da **for** $\alpha^* = 0.78$ **and** $\varepsilon = 0.9$

and the Nusselt number from

$$Nu = \frac{h_w(4H)}{k_f} = \frac{4}{k_1(\theta_{f,w} - \theta_{f,b})} \tag{69}$$

where 4H is the hydraulic diameter of the channel.

3.5 Nusselt Number for Interface Condition of Model B. Substituting Eqs. (25), (26), (49) and (51) in Eqs. (67) and (69), results in

$$Nu = \frac{h_w(4H)}{k_f} = \frac{4}{k_1\left[D_0(1-\eta_1)^4 + D_1(1-\eta_1)^3 + D_2(1-\eta_1)^2 + D_3(1-\eta_1) + \theta_f(\eta_1^-) - \theta_{f,b}\right]} \tag{70}$$

where

$$\theta_{f,b} = \frac{\theta_{f,pm} D_a \eta_1 + \theta_{f,om} U_{m,\text{open}}(1-\eta_1)}{U_m} \tag{71}$$

$$\theta_{f,pm} = \frac{\gamma}{(1+k)\lambda\sinh(\lambda\eta_1)}[\beta - k(1-\beta)]\left[\frac{\sinh(\lambda\eta_1)}{\lambda\eta_1 k} + \cosh(\lambda\eta_1)\right] - \frac{\gamma\eta_1}{3(1+k)} - \frac{\gamma}{(1+k)\eta_1 Bi} \tag{72}$$

$$\theta_{f,\,om} = \frac{1}{U_{m,\text{open}}}\left[-\frac{D_0}{14}(1-\eta_1)^6 + \left(\frac{-0.5D_1 + D_0D_9}{6}\right)(1-\eta_1)^5 + \left(\frac{-0.5D_2 + D_1D_9 + U_BD_0}{5}\right)(1-\eta_1)^4 + \left(\frac{-0.5D_3 + D_2D_9 + U_BD_1}{4}\right)(1-\eta_1)^3 + \left(\frac{-0.5\theta_f(\eta_1^-) + D_3D_9 + U_BD_2}{3}\right)(1-\eta_1)^2 + \left(\frac{\theta_f(\eta_1^-)D_9 + U_BD_3}{2}\right)(1-\eta_1) + \theta_f(\eta_1^-)U_B\right] \tag{73}$$

$$D_9 = \frac{\alpha^*}{\sqrt{Da}}(U_B - Da) \tag{74}$$

3.6 Nusselt Number for Interface Condition of Model A. The Nusselt number for interface condition of Model A can be obtained by substituting $\beta = \beta_{cr}$ in Eqs. (70)–(73).

3.7 Nusselt Number for Interface Condition of Model C. The Nusselt number for interface condition of Model C can be obtained by substituting $\beta = 1 - D_8 Bi_{\text{int}}\eta_1$ in Eqs. (70)–(73).

Since there are many parameters which will influence the heat transfer performance, a sensitivity analysis according to the Spearman Rank Correlation Coefficients method based on Monte Carlo sampling is implemented to show the relative importance of various parameters before discussing the Nusselt number results. As can be seen in Table 1, Da, η_1, and k have a strong influence on the Nusselt number; Bi, Bi_{int}, β, and ε have a moderate influence on the Nusselt number, while α^* has a weak influence on the Nusselt number. Figure 8 presents the variations of the Nusselt number for Model A. It is seen that, in general, the variations of Nusselt number as a function of η_1 can be divide into three stages. During the first stage, the Nusselt number increases as η_1 increases. After that, if η_1 continues to increase, the Nusselt number will drop. This can be referred to as the second stage. During the third stage, as η_1 increases further it will translate into the interface reaching almost to the wall. This will cause the Nusselt number to increase once again. The reason for the existence of these three stages can be explained using Figs. 9 and 10. Figure 9 presents the dimensionless velocity distributions as a function of η_1. Figure 10 present the variation of the maximum velocity at the open region for pertinent parameters η_1 and Da. It is found that, when the average velocity over the channel cross section is maintained unchanged, i.e., for the same Reynolds number, the maximum velocity at the open region will first increase and then decrease as η_1 increases from zero to one, while its location will move towards the wall. The heat transfer performance within the whole channel, which can be represented by the Nusselt number, is dependent on both the heat transfer characteristics of the porous region and that of the open region. During the first stage, an increase of the maximum velocity at the open region with η_1 results in a heat transfer enhancement at the open region. In the meantime, as shown in Fig. 4, since only a small amount of energy is transferred into the porous region, this will almost have no influence on the heat transfer performance within the porous region. Overall, this will result in an increase in Nusselt number. During the second stage, a decrease in the maximum velocity at the open region with η_1 results in a reduction in the heat transfer at the open region. Since only a relatively small amount of the imposed flux is transferred into the porous region, its influence on the heat transfer performance at the porous region is limited. Overall, this will result in a decrease in the Nusselt number. During the third stage, even though a drop in the maximum velocity within the open region will weaken the heat transfer at open region, there will be a heat transfer enhancement within the porous region because a large amount of energy is transferred by the porous medium, and the extensive interfacial area and tortuous flow passages within porous structure participate more actively in the heat exchange. Overall, this results in an increase in the Nusselt number. A large Da will increase the energy transferred by the porous region, and a large Bi will enhance the heat exchange

Table 1 Results of Spearman rank correlation coefficients test for sensitivity analysis (sampling size: 10^6)

Variable	Spearman rank correlation coefficient	p-Value	Rank
Da	−0.7843	0.00000	1
η_1	0.2446	0.00000	2
k	−0.1461	0.00000	3
Bi	0.0611	0.00000	4
Bi_{int} or β	0.0438	0.00000	5
ε	0.0220	0.00000	6
α^*	−0.0007	0.61187	7

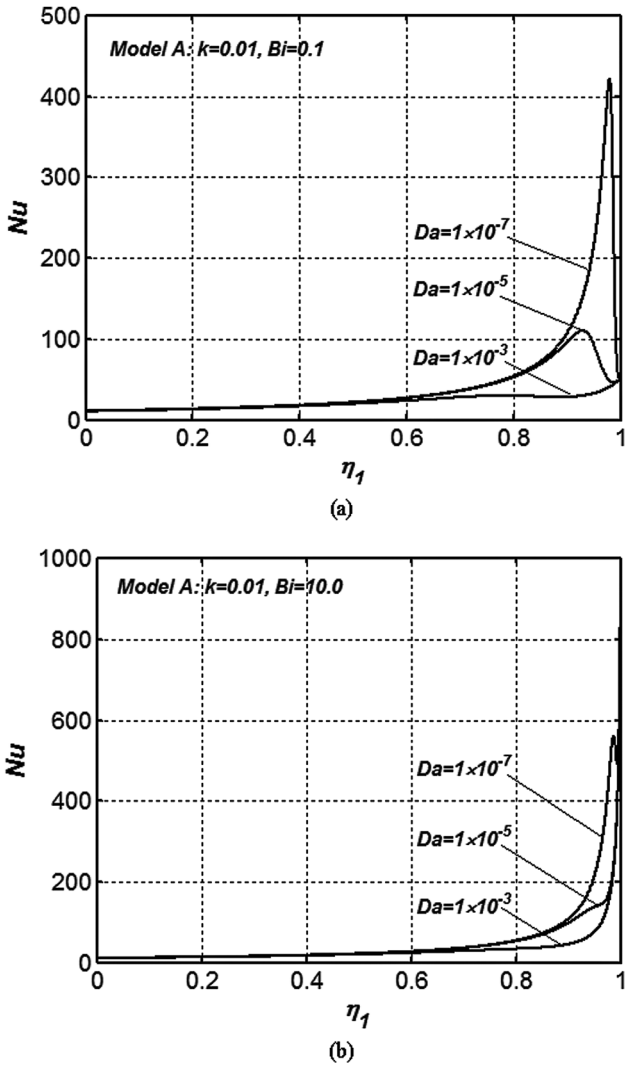

Fig. 8 Nusselt number variations as a function of pertinent parameters k, Bi, and Da for Model A for $\alpha^* = 0.78$ and $\varepsilon = 0.9$

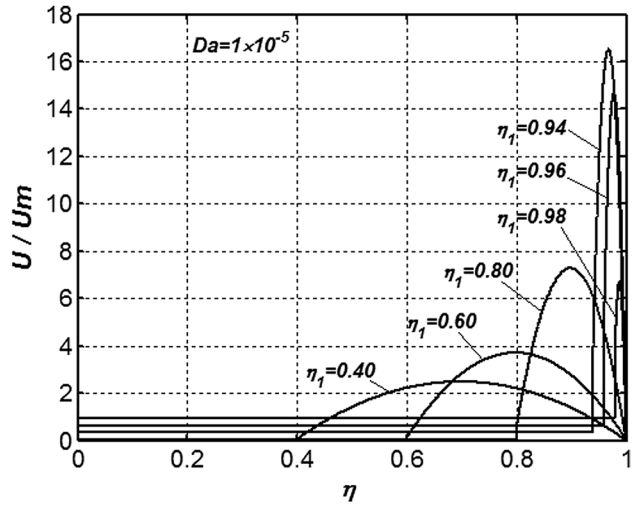

Fig. 9 Dimensionless velocity distributions as a function of η_1 for $\alpha^* = 0.78$

between the fluid and solid phases within the porous medium. As such the heat transfer within the porous region is enhanced and the second stage of the variation of the Nusselt number will disappear, such as the case of $Da = 1 \times 10^{-3}$ and $Bi = 10.0$, as shown in Fig. 8(*b*).

It is found that when $\alpha^* = 0$, and as $\eta_1 \to 0$, the Nusselt number will approach 8.235, which agrees well with the analytical solution for a smooth channel. On the other hand, as $\eta_1 \to 1$, the Nusselt number will become independent of Darcy number and is just dependent on the thermal condition at the porous-fluid interface. This is because that the fluid flow through the porous medium is represented by the Darcian flow model. Furthermore, if the Nusselt number is redefined as in Eq. (75) given below, which is the definition of Nusselt number used by Lee and Vafai [15], the Nusselt number calculated from Model A for $\eta_1 \to 1$ will approach that derived by them [15].

$$Nu = \frac{h_w(4H)}{k_{f,\text{eff}}} \tag{75}$$

The Nusselt number variations as a function of pertinent parameters k,Bi,Bi_{int}, and β for Models B and C are shown in Figs. 11

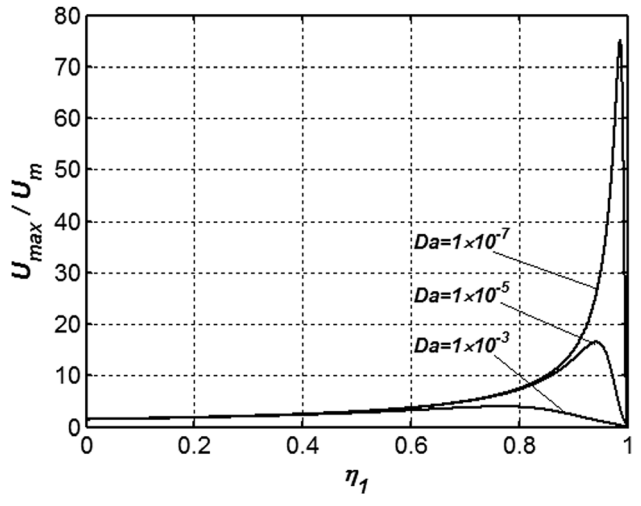

Fig. 10 The variation of the maximum velocity at the open region for pertinent parameters η_1 and *Da* for $\alpha^* = 0.78$

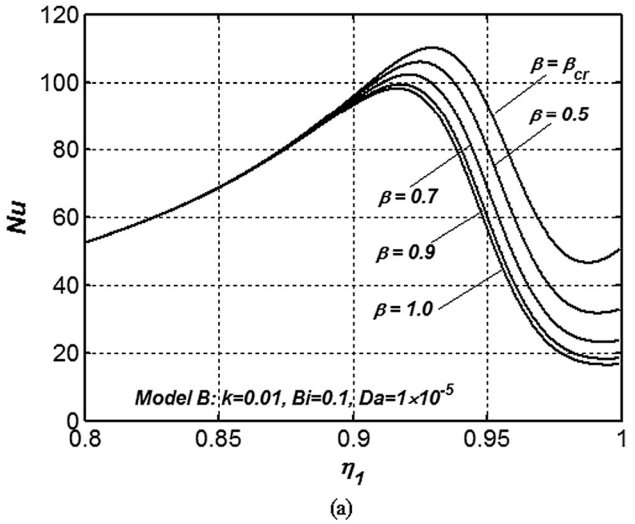

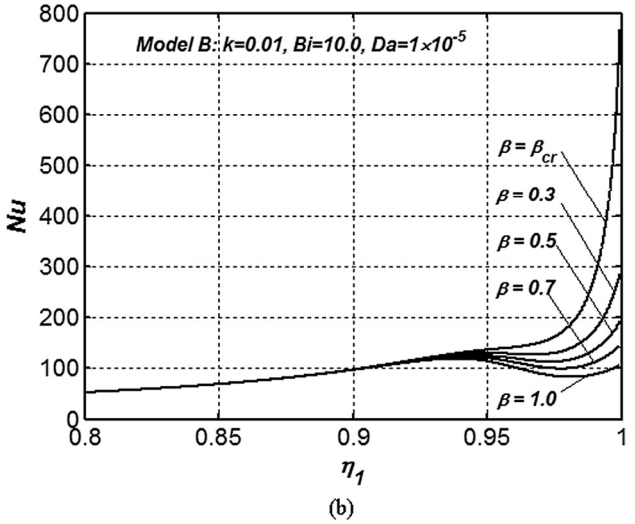

Fig. 11 Nusselt number variations as a function of pertinent parameters *k*,*Bi*, and β for Model B for $\alpha^* = 0.78$ and $\varepsilon = 0.9$

and 12, respectively. It should be noted that the Nusselt number calculated from Model B for $\beta = 1$ is also that calculated from Model C for $Bi_{\text{int}} = 0$; and the Nusselt number calculated from Model B for $\beta = \beta_{cr}$ is also that calculated from Model A as well as the one calculated from Model C for $Bi_{\text{int}} \to \infty$. When Bi_{int} becomes larger, or β becomes smaller, which will be translated into an enhanced heat transfer between the fluid and solid phases at the interface, more energy is transferred into the solid phase through interface. Since this energy is more effectively transferred through the porous structure, the Nusselt number will increase. When Model A is valid, the heat transfer between the fluid and solid phases at the interface has relatively the highest enhancement, thus the maximum fraction of the total heat flux at the interface will be transferred into the solid phase at the interface. Therefore, the Nusselt number calculated from Model A will be the largest among the three models. Furthermore, when Bi becomes larger, which translates into an enhanced internal heat transfer between the fluid and solid phases within the porous region, the Nusselt number will also increase. When k is large, a relatively smaller fraction of the imposed load will be transferred into the solid phase at the interface for any of the considered models, as seen in Fig. 2. As such, the thermal conditions at the porous-fluid interface will have almost no influence on the variations of Nusselt number, as shown in Figs. 12(*c*) and 12(*d*).

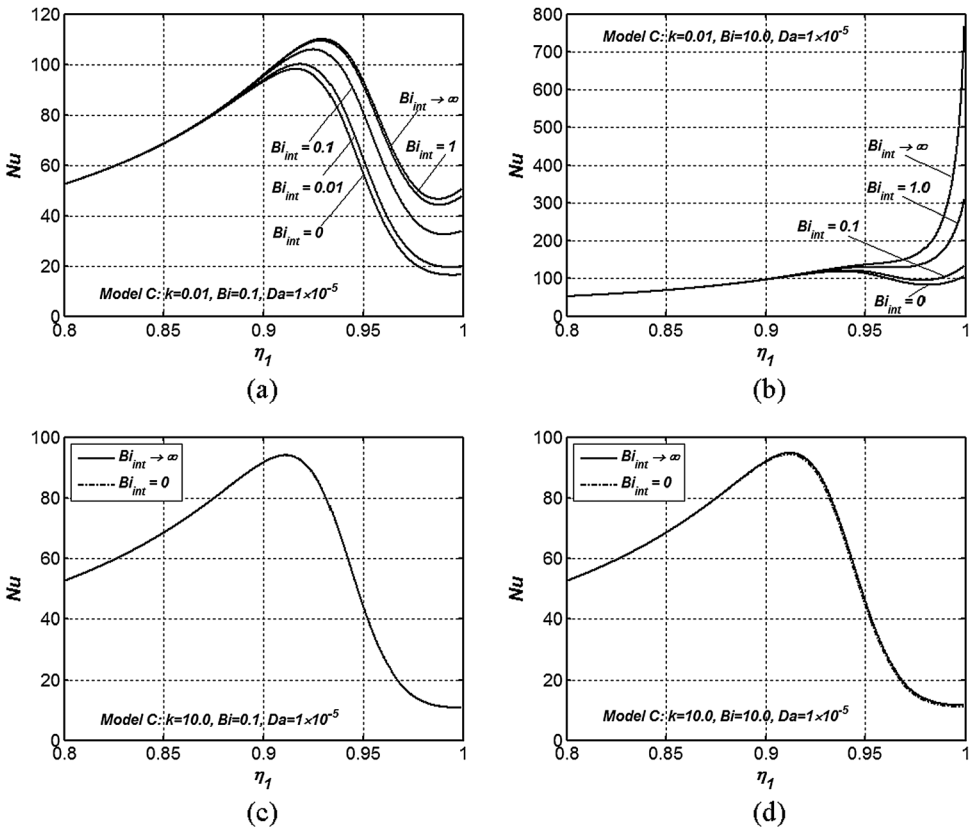

Fig. 12 Nusselt number variations as a function of pertinent parameters k,Bi, and Bi_{int} for Model C for $\alpha^* = 0.78$ and $\varepsilon = 0.9$

4 Conclusions

A comprehensive investigation of variant thermal conditions at the porous-fluid interface under LTNE condition is presented in this work. Exact solutions are derived for both the fluid and solid temperature distributions for five primary pertinent approaches (Models A, B.1, B.2, B.3, and C) for the porous-fluid interface. It is established in detail that the results obtained from these primary models can be transformed between each other. It is also found that the critical ratio of heat flux for the fluid phase to the total heat flux at the interface for Model B will provide the means for establishing its range of validity. The range of validity of all the models is analyzed in this work. Also a critical nondimensional half height of the porous media is determined, below which the LTE condition within porous region is considered to be valid. A comprehensive discussion of the three stages of variation of Nusselt number as a function of the height of porous media which is dependent on both the heat transfer characteristics of the porous region and that of open region is presented. Among the three interface thermal models, the Nusselt number calculated from Model A is shown to produce the largest values. Furthermore, the analytical results have been verified with several limiting cases. The agreement with the limiting cases is excellent.

Nomenclature

$Bi = Bi = \frac{h_i \alpha H^2}{k_{s,\text{eff}}}$, Biot number defined by Eq. (22)

$Bi_{\text{int}} = Bi_{\text{int}} = \frac{h_{\text{int}} H}{k_{s,\text{eff}}}$, interface Biot number defined by Eq. (22)

c_p = specific heat of the fluid, J kg^{-1} K^{-1}

$D_0, D_1, D_2, D_3, D_4, D_5, D_6, D_7, D_8$, and D_9, parameters calculated by Eqs. (45), (57), and (74)

$Da = Da = \frac{K}{H^2}$, Darcy number

h_i = interstitial heat transfer coefficient, W m^{-2} K^{-1}

h_{int} = interface heat transfer coefficient, W m^{-2} K^{-1}

h_w = wall heat transfer coefficient defined by Eq. (68), W m^{-2} K^{-1}

H = half height of the channel, m

H_1 = half height of the porous media, m

$k = k = \frac{k_{f,\text{eff}}}{k_{s,\text{eff}}}$, ratio of the fluid effective thermal conductivity to that of the solid

K = permeability, m^2

$k_1 = k_1 = \frac{k_f}{k_{s,\text{eff}}}$, ratio of the fluid thermal conductivity to the solid effective thermal conductivity

k_f = thermal conductivity of the fluid, W m^{-1} K^{-1}

$k_{f,\text{eff}}$ = effective thermal conductivity of the fluid, W m^{-1} K^{-1}

k_s = thermal conductivity of the solid, W m^{-1} K^{-1}

$k_{s,\text{eff}}$ = effective thermal conductivity of the solid, W m^{-1} K^{-1}

Nu = Nusselt number

p = pressure, N m^{-2}

q_i = heat flux at the interface, W m^{-2}

q_w = heat flux at the wall, W m^{-2}

T = temperature, K

u = fluid velocity, m s^{-1}

u_m = area average velocity over the channel cross section, m s^{-1}

$U = U = \frac{u}{-\frac{H^2}{\mu_f}\frac{dp}{dx}}$, dimensionless fluid velocity

U_B = dimensionless interface velocity

U_m = dimensionless average velocity over the channel cross section

x = longitudinal coordinate, m

y = transverse coordinate, m

Greek Symbols

α = interfacial area per unit volume of the porous medium, m^{-1}

α^* = velocity slip coefficient at the interface

ε = porosity

β = ratio of heat flux for the fluid phase to the total heat flux at the interface

$\beta_1, \beta_2, \beta_3$ = ratio of heat flux for the fluid phase to the total heat flux at the interface defined by Eq. (17)

$\eta = \eta = \frac{y}{H}$, nondimensional transverse coordinate

$\eta_1 = \eta_1 = \frac{H_1}{H}$, nondimensional half height of the porous media

$\theta = \theta = \frac{k_{s,\text{eff}}(T - T_{s,i})}{q_w H}$, nondimensional temperature, defined by Eq. (22)

μ = dynamic viscosity [kg m^{-1} s^{-1}]

ρ = density [kg m^{-3}]

$\gamma = \gamma = \frac{q_i}{q_w}$, dimensionless heat flux at the interface

$\lambda = \lambda = \sqrt{Bi(1+k)/k}$, parameter calculated by Eq. (43)

ρ = fluid density, kg m^{-3}

Subscripts

b = bulk mean value

cr = critical value

f = fluid

i = interface

$open$ = open region

p = porous region

s = solid phase

w = wall

References

[1] Poulikakos, D., and Kazmierczak, M., 1987, "Forced Convection in A Duct Partially Filled With A Porous Material," ASME J. Heat Transfer, **109**, pp. 653–662.

[2] Chikh, S., Boumedien, A., Bouhadef, K., and Lauriat, G., 1995, "Analytical Solution of Non-Darcian Forced Convection in An Annular Duct Partially Filled With A Porous Medium," Int. J. Heat Mass Transfer, **38**(9), pp. 1543–1551.

[3] Alkam, M. K., and Al-Nimr, M. A., 1999, "Improving the Performance of Double-Pipe Heat Exchangers by Using Porous Substrates," Int. J. Heat Mass Transfer, **42**(19), pp. 3609–3618.

[4] Mohamad, A. A., 2003, "Heat Transfer Enhancements in Heat Exchangers Fitted With Porous Media Part I: Constant Wall Temperature," Int. J. Thermal Sci., **42**(4), pp. 385–395.

[5] Pavel, B. I., and Mohamad, A. A., 2004, "An Experimental and Numerical Study on Heat Transfer Enhancement for Gas Heat Exchangers Fitted With Porous Media," Int. J. Heat Mass Transfer, **47**(23), pp. 4939–4952.

[6] Kim, W. T., Hong, K. H., Jhon, M. S., VanOsdol, J. G., and Smith, D. H., 2003, "Forced Convection in a Circular Pipe With a Partially Filled Porous Medium," J. Mech. Sci. Technol., **17**(10), pp. 1583–1595.

[7] Satyamurty, V. V., and Bhargavi, D., 2010, "Forced Convection in Thermally Developing Region of a Channel Partially Filled With a Porous Material and Optimal Porous Fraction," Int. J. Therm. Sci., **49**(2), pp. 319–332.

[8] Kuznetsov, A. V., 2000, "Analytical Studies of Forced Convection in Partly Porous Configurations," *Handbook of Porous Media*, K. Vafai, ed., Dekker, New York, pp. 269–312.

[9] Beavers, G. S., and Joseph, D. D., 1967, "Boundary Conditions at a Naturally Permeable Wall," J. Fluid Mech., **30**(1), pp. 197–207.

[10] Vafai, K., and Thiyagaraja, R., 1987, "Analysis of Flow and Heat Transfer at the Interface Region of a Porous Medium," Int. J. Heat Mass Transfer, **30**, pp. 1391–1405.

[11] Vafai, K., and Kim, S., 1990, "Fluid Mechanics of the Interface Region Between a Porous Medium and a Fluid Layer—An Exact Solution," Int. J. Heat Fluid Flow, **11**, pp. 254–256.

[12] Alazmi, B., and Vafai, K., 2001, "Analysis of Fluid Flow and Heat Transfer Interfacial Conditions Between a Porous Medium and a Fluid Layer," Int. J. Heat Mass Transfer, **44**, pp. 1735–1749.

[13] Amiri, A., and Vafai, K., 1994, "Analysis of Dispersion Effects and Non-Thermal Equilibrium Non-Darcian, Variable Porosity Incompressible Flow Through Porous Medium," Int. J. Heat Mass Transfer, **37**, pp. 939–954.

[14] Amiri, A., and Vafai, K., 1998, "Transient Analysis of Incompressible Flow Through a Packed Bed," Int. J. Heat Mass Transfer, **41**, pp. 4259–4279.

[15] Lee, D. Y., and Vafai, K., 1999, "Analytical Characterization and Conceptual Assessment of Solid and Fluid Temperature Differentials in Porous Media," Int. J. Heat Mass Transfer, **42**, pp. 423–435.

[16] Marafie, A., and Vafai, K., 2001, "Analysis of Non-Darcian Effects on Temperature Differentials in Porous Media," Int. J. Heat Mass Transfer, **44**, pp. 4401–4411.

[17] Alazmi, B., and Vafai, K., 2002, "Constant Wall Heat Flux Boundary Conditions in Porous Media Under Local Thermal Non-Equilibrium Conditions," Int. J. Heat Mass Transfer, **45**, pp. 3071–3087.

[18] Ochoa-Tapia, J. A., and Whitaker, S., 1997, "Heat Transfer at the Boundary Between a Porous Medium and a Homogeneous Fluid," Int. J. Heat Mass Transfer, **40**(11), pp. 2691–2707.

[19] Narasimhan, A., and Reddy, B. V. K., 2011, "Laminar Forced Convection in a Heat Generating Bi-Disperse Porous Medium Channel," Int. J. Heat Mass Transfer, **54**(1–3), pp. 636–644.

[20] Yang, Y. T., and Hwang, M. L., 2009, "Numerical Simulation of Turbulent Fluid Flow and Heat Transfer Characteristics in Heat Exchangers Fitted With Porous Media," Int. J. Heat Mass Transfer, **52**(13–14), pp. 2956–2965.

[21] Yang, Y. T., and Hwang, M. L., 2008, "Numerical Simulation of Turbulent Fluid Flow and Heat Transfer Characteristics in a Rectangular Porous Channel With Periodically Spaced Heated Blocks," Numer. Heat Transfer; Part A, **54**(8), pp. 819–836.

[22] Jeng, T. M., 2008, "A Porous Model for the Square Pin-Fin Heat Sink Situated in a Rectangular Channel with Laminar Side-Bypass Flow," Int. J. Heat Mass Transfer, **51**, pp. 2214–2226.

[23] Yucel, N., and Guven, R., 2007, "Forced Convection Cooling Enhancement of Heated Elements in a Parallel Plate Channels Using Porous Inserts," Numer. Heat Transfer, Part A, **51**, pp. 293–312.

[24] Zahmatkesh, I., and Yaghoubi, M., 2006, "Studies on Thermal Performance of Electrical Heaters by Using Porous Materials," Int. Commun. Heat Mass Transfer, **33**(2), pp. 259–267.